

Growth Stage Kinetics in the Synthesis of Al₂O₃/Al Composites by Directed Oxidation of Al–Mg and Al–Mg–Si Alloys

H. Venugopalan & T. DebRoy*

Department of Materials Science and Engineering, Pennsylvania State University, University Park, PA 16802, USA

(Received 20 August 1995; revised version received 18 March 1996; accepted 28 March 1996)

Abstract

Although synthesis of ceramic matrix composites by the directed oxidation process offers significant advantages over traditional composite processing routes, the scientific basis for the process is not fully understood. This paper is addressed to understanding the mechanism of composite growth from Al–Mg and Al–Mg–Si alloys theoretically and experimentally. Analysis of the oxidation kinetics of Al–Mg and Al–Mg–Si alloys for various oxygen pressures, temperatures and durations of oxidation, obtained in this study and reported in the literature, demonstrates that the growth kinetics can be tailored by the control of alloy composition. For the Al–Mg alloys, transport of oxygen through a thin alloy layer near the surface controls the growth rate. When Si is added to the alloy, the oxidation mechanism is completely changed. The rate of oxidation of Al–Mg–Si alloys depends on the transport of electronic species through a thin MgO layer at the top surface of the composite. Apart from contributing to a more complete understanding of the growth stage, the mechanism of composite growth will serve as a basis for improving growth rates.

© 1996 Elsevier Science Limited

Introduction

In the directed melt oxidation (DIMOX) process, a molten aluminium alloy is oxidized to produce ceramic/metal composites.¹ Figure 1 illustrates schematically the formation of composite materials in this process. Under appropriate conditions of alloy composition, temperature and oxygen pressure, a rapid reaction of the molten alloy with the oxidant to form α -alumina occurs and the reaction

product grows outwards from the original metal surface. The reaction is fed by transport of liquid metal through the reaction product.¹ The resulting material is an Al₂O₃/Al composite with an interconnected network of unoxidized metal.² Reinforced composites with the desired structural properties can be obtained by growing the 'composite' matrix into preforms consisting of reinforcing particulates, whiskers or fibres of Al₂O₃, SiC, etc.^{3–5} Composites made by directed oxidation can be tailored to have good toughness, thermal shock resistance, wear resistance, high stiffness, and high temperature stability. They are being used or evaluated for use in turbine engine components, armour applications, heat exchangers and furnace components.⁶ Several ceramic composite systems based on the directed metal oxidation technology have been developed, as listed in Table 1.³

It is now recognised that the presence of volatile elements like Mg or Zn is crucial for directed oxidation of aluminium alloys to take place.^{1,7} Dopants like Mg or Zn are believed to hinder the formation of a protective alumina film on the alloy surface and thus allow continued oxidation of the alloy. Additional elements such as Si are usually added to improve alloy/preform compatibility. These dopants can be either applied to the surface of the aluminium exposed to the oxidant or, if soluble, alloyed with the parent metal. Three distinct stages can be observed in the oxidation of Al–Mg alloys at a given temperature⁸ (Fig. 2). When Al–Mg alloys are heated in argon to a given temperature and then exposed to an oxygen atmosphere, an initial stage of rapid weight gain occurs.⁸ During this period, MgO forms by oxidation of Mg vapour and subsequently falls back on to the melt surface.⁹ Formation of a dense, thin layer of MgAl₂O₄ beneath the MgO halts the initial stage of oxidation and corresponds to the start of incubation.⁸ During incubation, metal

*To whom correspondence should be addressed.

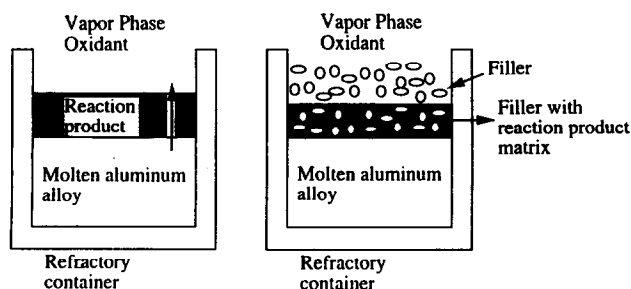


Fig. 1. Schematic description of formation of ceramic matrix composites by the directed oxidation process.

channels are observed to form in the spinel. The arrival of these metal channels at the top of the spinel is believed to correspond to the end of incubation and the start of the growth stage.¹⁰ Composite formation in the growth stage starts when the near-surface aluminum alloy becomes depleted in Mg and reaches a concentration where Al_2O_3 formation becomes more favourable than MgAl_2O_4 .¹⁰ During growth, bulk oxidation of Al to Al_2O_3 occurs epitaxially on the spinel.¹¹

Several models have been proposed to explain the kinetics of oxidation of Al to Al_2O_3 in the growth stage.^{8,12} It has been suggested that during the growth stage of directed oxidation of Al-Mg alloys, a continuous MgO film exists at the top of the alumina matrix with a thin aluminium alloy film separating the two layers^{11,13} (Fig. 3). The presence of this continuous MgO film restricts the formation of a protective alumina layer on the surface. At the MgO/Al-alloy film interface, MgO dissociates and oxygen dissolves in the Al-alloy film. The magnesium ions formed by dissociation of MgO diffuse through the MgO layer to the MgO/air interface where they are oxidized to regenerate MgO. During the outward transport of magnesium ions through MgO, electrical neutrality is maintained by the simultaneous transport of electronic defects.¹² The oxygen dissolved in the alloy film is transported, from the MgO/alloy film interface, to the alloy film/ Al_2O_3 interface where composite growth takes place epitaxially. The supply of aluminium to the alloy film/ Al_2O_3 interface is thought to be sustained by the wicking of metal

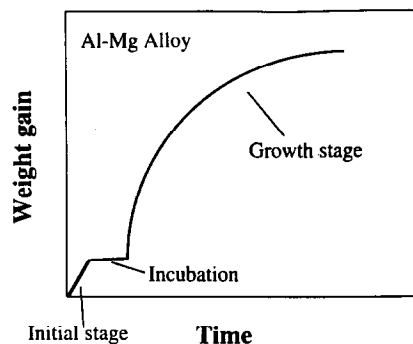


Fig. 2. Schematic plot of weight gain as a function of time for directed oxidation of Al-Mg alloys.

through channels in the alumina. One or more of the above-mentioned reaction steps could be the rate-controlling mechanism in the growth stage.

Nagelberg *et al.*¹² conducted directed oxidation studies of Al-Mg alloys to which Si was added. According to Nagelberg *et al.*,¹² the rate of oxidation of Al-Mg-Si alloys in the growth stage is controlled by the electronic conductivity of the continuous, external, MgO layer. To investigate the role of electronic transport in the oxidation kinetics in the growth stage, DebRoy *et al.*¹⁴ carried out directed oxidation experiments of an Al-Mg alloy (Al-5056 alloy) in which platinum wires were positioned inside the alloy so that the wires would extend through the composite matrix and the top MgO layer to facilitate electronic transport. They¹⁴ observed that the rate of oxidation in the growth stage was independent of the presence or absence of Pt wires, indicating that the transport of electronic species does not control the oxidation kinetics of Al-Mg alloys that do not contain silicon. Thus, in the absence of silicon, electronic transport through the MgO layer is no longer the rate-controlling mechanism in the growth stage of Al-Mg alloys. In view of the crucial difference in the oxidation mechanism of Al-Mg alloys with or without the presence of Si, the role of silicon in the mechanism of composite growth from Al-Mg alloys needs to be investigated in detail.

In this paper, we examine the directed oxidation of Al-Mg and Al-Mg-Si alloys experimentally and theoretically. The oxidation kinetics are studied by thermogravimetry. The weight gain in the growth stage is monitored as a function of oxygen pressure, time and temperature. By analysing the experimental results reported in this paper and the available independent results in the literature, the role of silicon in the rate of composite growth is investigated. We show that the oxygen transport in the near-surface alloy layer controls the rate of alumina formation in the growth stage of directed oxidation of binary Al-Mg alloys. Analysis of the influence of silicon on the various steps in the growth

Table 1. Example of Lanxide^{®a} ceramic matrix systems³

Parent metal	Reaction product
Al	Oxide, nitride, boride, titanate
Si	Nitride, boride, carbide
Ti	Nitride, boride, carbide
Zr	Nitride, boride, carbide
Hf	Boride, carbide
Sn	Oxide
La	Boride

^aLanxide[®] is a registered trademark of Lanxide Corporation, DE, USA.

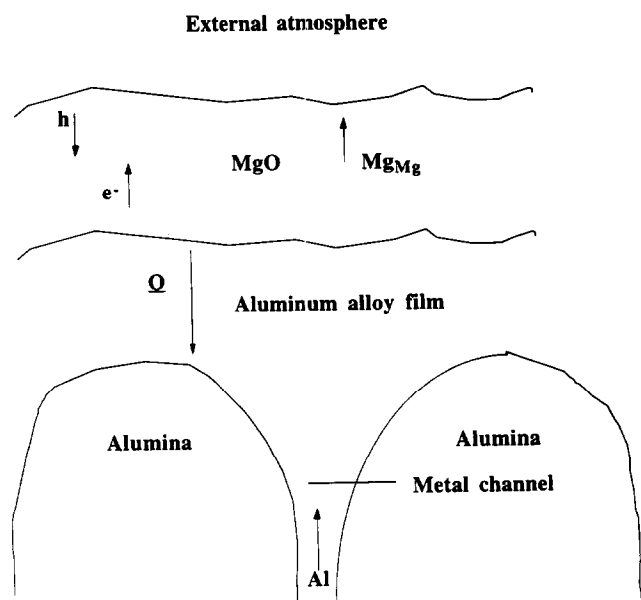


Fig. 3. Schematic diagram of the composite structure. Mg_{Mg} denotes a magnesium ion on the cationic site in MgO , and h denotes a hole.

stage indicates that silicon additions increase the rate of oxygen transport through the alloy layer and decrease the rate of electronic transport through the MgO layer. As a result, electronic transport through the outer MgO layer controls the rate of oxidation of Al–Mg–Si alloys.

Experimental Procedure

The thermogravimetric set-up, used for studying reaction kinetics in the directed oxidation of Al–Mg alloys, consisted of a Cahn model 1000 automatic recording electric balance, a high-temperature silicon carbide tube furnace, and a gas flow and pressure control system. A schematic diagram of the experimental set-up is shown in Fig. 4. The balance had a sensitivity of $0.5 \mu g$ and the measurement accuracy was 0.1% of the range. The quartz reaction tube was of 48 mm internal diameter and had a 25 mm equi-temperature zone at the centre of the furnace. The furnace was equipped with an electronic temperature controller which regulated the temperature to ± 5 K.

A cylindrical sample, 14 mm in diameter and 8 mm in length, of an Al 5056 alloy (5 wt% Mg, 0.10 wt% Cu, 0.40 wt% Fe, 0.10 wt% Zn, 0.10 wt% Mn and balance Al) was placed in an alumina crucible, 14.2 mm in diameter and 27 mm in length. SiO_2 powder (99.9%, –325 mesh) was added to the surface of some samples as Si source. A previous investigation¹⁵ of the kinetics of reaction between SiO_2 and molten aluminium revealed that SiO_2 is completely reduced by the aluminium melt during initial heating to the test temperature (>1350 K), which takes about an hour. Thus, SiO_2

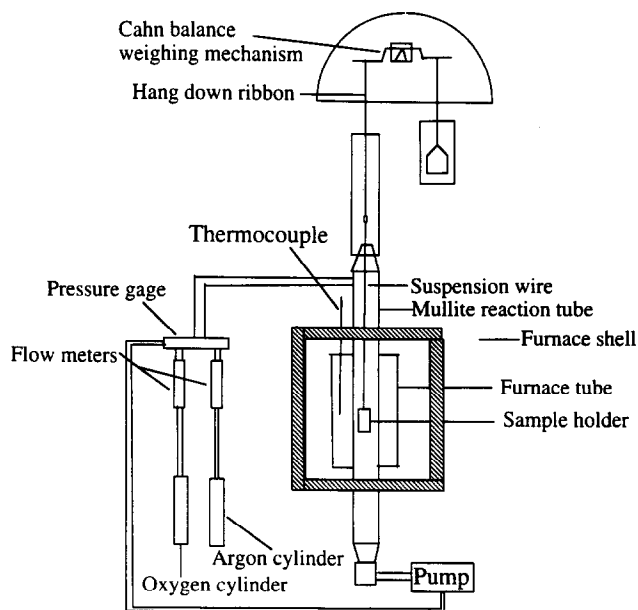


Fig. 4. Schematic diagram of the thermogravimetric set-up.

additions of 205 mg effectively result in a composition of 3.3 mol% Si in the alloy. The crucible, containing the alloy, was suspended by a platinum wire from the balance and positioned within the equi-temperature zone of the furnace. Prior to conducting each experiment, the reaction tube was evacuated and purged with argon. The samples were then heated to the test temperature at a heating rate of 0.33 K s^{-1} in a pure argon atmosphere. When the target temperature was reached, a mixture of ultrahigh purity oxygen and argon was introduced at predetermined flow rates with the help of mass flow controllers, to obtain a target gas composition. Oxidation experiments were conducted at various partial pressures of oxygen, and reactor temperatures. Experiments were done at a constant total pressure of 93.3 kPa. Experiments were repeated to check the reproducibility of the weight gain data. The total gas flow rate was kept constant at $8333 \text{ mm}^3 \text{ s}^{-1}$ STP (298 K and 101.3 kPa). A typical scatter of 1–5% was observed in the weight gain measured during oxidation. The weight of the sample was continuously recorded using a computer data acquisition system. Subsequently, the recorded data were differentiated numerically to obtain the weight gain rate. The zero of the time axis is when oxygen of the desired partial pressure is introduced in the reactor. It takes about 75 s for the gas to reach the crucible. No correction of the zero of the time axis was made since the total oxidation time is of the order of about 60 ks. The internal cross-sectional area of the crucible, 154 mm^2 , was used for the calculation of reaction rates.

In the directed oxidation of binary Al–Mg alloys, the oxidation product, Al_2O_3 , often grew along the crucible walls in the growth stage. The behaviour

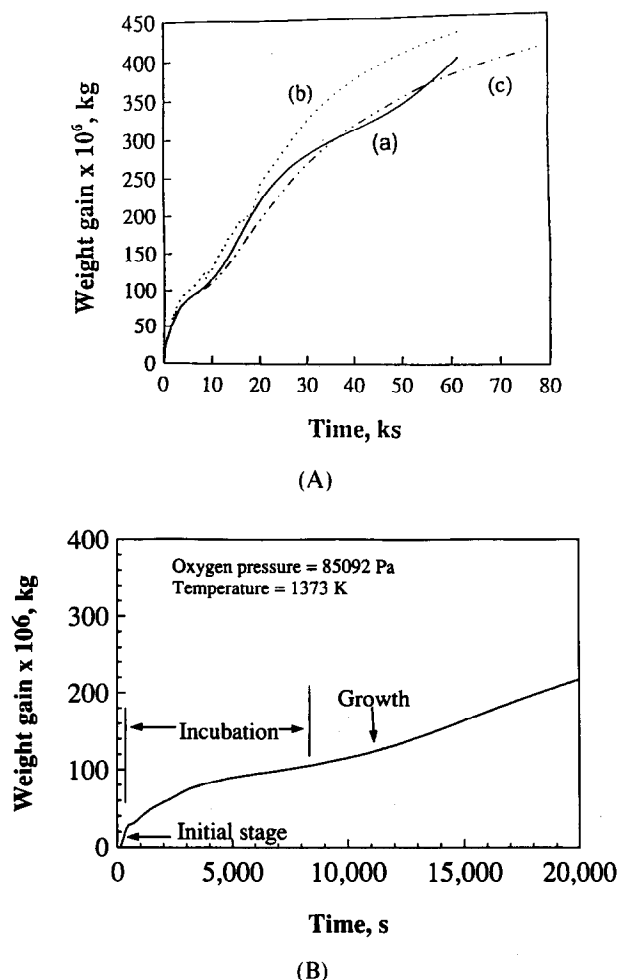


Fig. 5. (A) Weight gain versus time for the Al-Mg alloy at different oxygen pressures in the growth stage: (a) 85 092 Pa, (b) 21 273 Pa and (c) 42 546 Pa. The oxygen pressure was initially maintained at 85 092 Pa and subsequently changed in the growth stage. The total pressure, temperature and the total gas flow rate were maintained constant at 93 303 Pa, 1373 K and 8333 mm³ s⁻¹ STP, respectively. (B) Weight gain versus time for the Al-Mg alloy, at 1373 K and oxygen pressure of 85 092 Pa, at short oxidation times.

is similar to the preferential growth of alumina on the crucible wall observed by Xiao and Derby¹⁶ and Manor *et al.*¹⁷ The creeping is not surprising since the MgO which forms in the gas phase coats the crucible walls.⁹ MgO is unstable in the presence of the Al-5 wt% Mg alloy at the temperatures involved in directed oxidation.¹⁸⁻²⁰ Therefore, there is a net driving force for the reaction between Al and MgO. The reaction causes Al to wet MgO,²¹ creep along the walls and react with oxygen in the external atmosphere to form alumina. The metal creeping leads to a change in the melt cross-sectional area exposed to the oxygen atmosphere with time and complicates study of reaction kinetics. Investigation of initial stage kinetics⁹ reveals that higher the oxygen pressure, the lower the total amount of MgO formed in the initial stage. Hence to minimize creeping in the directed oxidation of binary Al-Mg alloys, the oxygen pressure in the

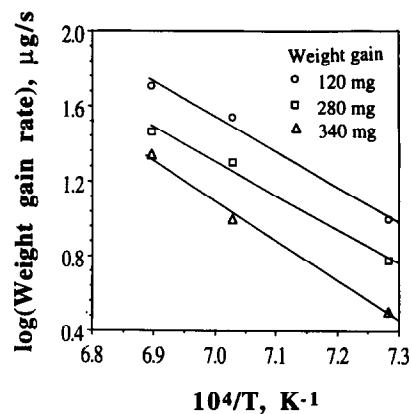


Fig. 6. Weight gain rate versus temperature for Al-Mg alloy for an oxygen pressure of 85 092 Pa, for different weight gains. The computed activation energies were 357.9, 345.9 and 407.8 kJ mol⁻¹ for 120, 280 and 350 mg weight gains, respectively. The total pressure and the total gas flow rate were maintained constant at 93 303 Pa and 8333 mm³ s⁻¹ STP, respectively.

initial stage and in the incubation period was kept at a high value of 85.1 kPa and the oxygen pressure was subsequently changed in the growth stage. The end of incubation was identified from the weight gain data (in the course of the experiment) as the time at which there is an increase in the weight gain rate.

Results and Discussion

A typical weight gain versus time curve observed in the directed oxidation of Al-Mg alloys is shown in Fig. 2. The process starts with a rapid but limited oxidation event upon introduction of oxygen in the furnace. The initial oxidation, corresponding to the formation of MgO, ends abruptly with the formation of an MgAl₂O₄ film on the alloy surface. This event is followed by an incubation period where the weight gain is small. The onset of bulk growth is marked by a substantial increase in the oxidation rate. The kinetics and mechanism of the growth stage of composite synthesis from Al-Mg alloys, with or without silicon, are discussed in the following sections.

Mechanism of oxidation of Al-Mg alloys in the growth stage

Figure 5(A) is a plot of weight gain versus time for Al-Mg alloys for oxygen pressure of 85.1 kPa in the initial and incubation stages and varying oxygen pressures in the growth stage. It is observed that the oxidation rate in the growth stage decreases with time and, within experimental uncertainty, remains practically independent of oxygen pressure. Figure 5(B) is a plot of weight gain versus time at short oxidation times. Three different stages in the oxidation plot can be distinguished. Weight gain,

as a function of time, was also measured at various temperatures (1373–1450 K) for an oxygen pressure of 85.1 kPa. The weight gain rates in the growth stage, for different weight gains, were measured from the slopes and are plotted in Fig. 6. (Note that, for parabolic kinetics, weight gain rate measured at a constant weight gain would be proportional to the rate constant. The temperature dependence of the rate constant gives the activation energy.) Several important questions arise from the perusal of the rate data. Why does the weight gain rate decrease with time? Why is the weight gain rate practically independent of oxygen pressure? What is the rate-controlling mechanism in the growth stage of directed oxidation of Al-Mg alloys?

As shown in Fig. 3, the composite structure near the growth surface^{11–13} consists of a continuous Al₂O₃-doped MgO layer on top of the alumina matrix with a thin aluminium alloy film separating the two layers. At the MgO/Al-alloy film interface, MgO dissociates, and the oxygen dissolves in the alloy film and is transported to the Al₂O₃/Al-alloy film interface where composite growth takes place epitaxially. The magnesium ions formed by the dissociation of MgO diffuse through the MgO layer to the MgO/air interface where they are oxidized to regenerate MgO. This ionic transport is accompanied by electronic conduction (holes or electrons) to maintain charge neutrality and is taken to be the rate-limiting process in the regeneration of MgO.¹² The supply of liquid aluminium to the alloy film/alumina interface is sustained by wicking of metal through channels in the alumina. Thus, the three possible rate-controlling steps in the growth of Al₂O₃/Al composites from Al-Mg alloys are: (i) electronic transport through the external MgO layer, (ii) transport of liquid metal by capillarity through the interconnected metal channels in the alumina, and (iii) dissociation of MgO and the subsequent transport of oxygen from the MgO/alloy film interface to the Al₂O₃/alloy film interface.

The existence of long columns of composite containing Al₂O₃ grains of similar orientation^{11,13} disqualifies any process involving repeated nucleation of grains. This indicates that the growth process is continuous. Indeed, it can be observed from the composite macrostructure (Fig. 7) that the growth surface on the whole is macroscopically smooth. Hence, a one-dimensional model can be used to theoretically estimate the rates of the various transport processes involved in Al₂O₃ growth. The experimental results in Figs 5 and 6 are analysed below in detail to determine which of the above-mentioned steps are consistent with the observed growth rate and its dependence on time, oxygen pressure and temperature.

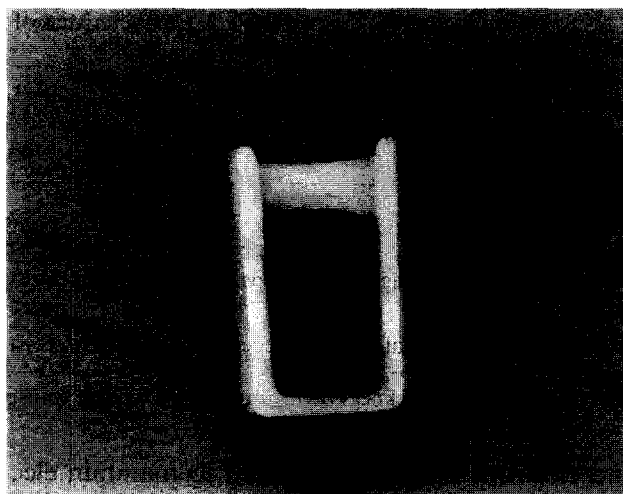
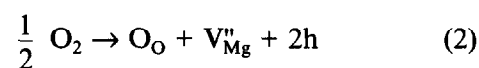


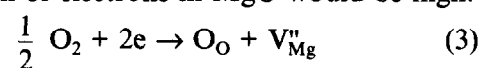
Fig. 7. Macrograph of composite (top region of crucible) grown from Al-5 wt% Mg alloy (bottom region of crucible).

Electronic transport through MgO

Since MgO is unstable for the alloy compositions typically used in directed oxidation,^{18–20} MgO dissociates at the alloy film/MgO interface to give up oxygen which is subsequently transported to the Al₂O₃/alloy film interface. The MgO could be regenerated either by the outward diffusion of magnesium ions to the external surface or by the inward diffusion of oxygen ions from the MgO/air interface to the MgO/alloy film interface (Fig. 3). According to Nagelberg *et al.*,¹² transport through the MgO layer is controlled by grain boundary diffusion of magnesium ions. This ionic transport is accompanied by electronic conduction (holes or electrons) to maintain charge neutrality and is taken to be the rate-limiting process. Near the external surface, in the Al₂O₃-doped MgO, holes are the dominant electronic defect and their concentration is proportional to $P_{O_2}^{1/4}$, where P_{O_2} is the partial pressure of oxygen in the reaction chamber.¹² This behaviour follows from the following defect reactions for the dissolution of alumina and oxygen in MgO:



where V_{Mg}'' denotes a magnesium ion vacancy, $\text{Al}_{\text{Mg}}^{\bullet}$ represents the dissolved aluminium concentration in MgO and h indicates a hole. Similarly, for the low oxygen pressures near the alloy film, the concentration of electrons in MgO would be high.



Thus, the outward transport of magnesium ions in the MgO towards the external surface is accompanied by the transport of holes near the external surface

Table 2. Characteristics of various events in the growth stage

Event	Oxygen pressure dependence of growth rate	Time dependence of growth rate	Activation energy (kJ mol ⁻¹)	Weight gain rate (mg cm ⁻² h ⁻¹) at 1373 K
Magnesium ion flux	$P_{O_2}^{1/4}$	Independent of time	310	17.44
Liquid metal transport	Independent of oxygen pressure	Decreases with time	6.1	6415
Oxygen transport through alloy film	Independent of oxygen pressure	Decreases with time	243.6	53.17 ^a
Experimental growth rate	Independent of oxygen pressure	Decreases with time	361	12.75

^aFor an alloy layer thickness of 12 μm , rate of oxygen transport is 13.39 mg cm⁻² h⁻¹.

and electrons near the alloy film to maintain electrical neutrality. From reaction (2), the hole concentration, p , is given as:

$$p = \left[\frac{K}{V_{\text{Mg}}''} \right]^{1/2} P_{O_2}^{1/4} \quad (4)$$

where K is the equilibrium constant of reaction (2).

From charge neutrality, we have:

$$V_{\text{Mg}}'' = \frac{1}{2} Al_{\text{Mg}}^* \quad (5)$$

The flux of magnesium ions and the corresponding flux of oxygen is proportional to the hole concentration, p .¹² Following the procedure of Nagelberg *et al.*,¹² the oxygen flux, J , in g cm⁻² s⁻¹, at 1373 K, is given as:

$$J \propto \left[\frac{K}{V_{\text{Mg}}''} \right]^{1/2} P_{O_2}^{1/4} = 3.15 \times 10^6 P_{O_2}^{1/4} \exp\left(\frac{-310 \times 10^3}{RT}\right) \quad (6)$$

where P_{O_2} is the partial pressure of oxygen in atmospheres, R is the gas constant in J mol⁻¹ K⁻¹, and T is the temperature in K. The activation energy for the process is 310 kJ mol⁻¹ which corresponds to the mobility of holes in MgO (Table 2).

Oxygen pressure and time dependences of magnesium ion transport. It is seen from eqn (6) that if magnesium ion flux through MgO were rate-limiting, the oxygen flux (growth rate) would exhibit a $P_{O_2}^{1/4}$ dependence. Thus eqn (6) predicts that, for a change in oxygen pressure from 21.3 to 85.1 kPa, the weight gain rate would increase by 41.4%. However, a 6.5% decrease in the weight gain rate is observed in the average experimental growth rate (Fig. 5) when the oxygen pressure is changed from 21.3 to 85.1 kPa. Equation (6) also predicts that the oxygen flux should be independent of time. Experimentally, however, the weight gain rate (growth rate) decreases with time. Thus, this mechanism cannot explain either the manner in which the rate varies with time or the observed effect of oxygen pressure on the growth rate. Therefore, this event is ruled out as a rate-limiting step.

Liquid metal transport

Rate expression. The reaction of Al with oxygen to form Al₂O₃ requires the continued supply of aluminium to the Al-alloy film/Al₂O₃ interface. This is believed to occur via convective flow of metal by wicking (capillary action) through the thickening Al₂O₃ reaction product via the interconnected metal channels. If liquid metal transport through metal channels is rate-controlling, the total metal flow through the channels would determine the composite growth rate. Furthermore, the growth rate will show the same dependence on time and P_{O_2} as capillary flow. Therefore, the time and P_{O_2} dependences of metal flow rate and the corresponding oxygen weight gain rate need to be analysed. As shown in Appendix A, the weight gain rate per unit area, J , is given by:

$$J = \frac{48}{54} \frac{f \rho_{\text{Al}} R \gamma_{\text{LV}} \cos \theta}{4 \mu x} \quad (7)$$

$$= \frac{48}{54} \frac{f \rho_{\text{Al}}}{4} \left[\frac{2R \gamma_{\text{LV}} \cos \theta}{\mu t} \right]^{1/2}$$

where f is the total metal channel area per unit area of the composite, ρ_{Al} the density of molten aluminium alloy, R is the radius of the channel, γ_{LV} is the surface tension of the molten alloy, θ is the contact angle between the molten alloy and alumina, μ is the viscosity of the molten alloy, x is the thickness of the composite, and t is the time of oxidation.

Oxygen pressure and time dependences of rate of liquid metal transport. It is seen from eqn (7) that if liquid metal transport is rate-controlling, the growth rate would be independent of oxygen pressure and decrease with time. The experimentally observed oxygen pressure and time dependences of rate (Fig. 5) are qualitatively consistent with that predicted by eqn (7) for liquid metal transport. If the predicted growth rate is also in good agreement with the experimentally observed growth rate for the Al-5 wt% Mg alloy, transport of liquid metal can then be considered as the rate-controlling step in the growth of Al₂O₃/Al composites.

Table 3. Data used for the calculation of rate of liquid metal transport

Property	Symbol	Value	Ref.
Total metal channel area per unit area of the composite	f	10^{-5}	2
Density of aluminium (kg m ⁻³)	ρ_{Al}	2300	22
Channel radius (m)	R	3×10^{-6}	11
Viscosity of molten aluminium (N s m ⁻²)	μ	6.21×10^{-4}	23
Vapour pressure of magnesium (N m ⁻²)	P_c	5019	18–20
Gravitational pressure (N m ⁻²)	P_g	2955 ^a	This study
Capillary pressure (N m ⁻²)	P_v	6.3×10^5	Appendix A

^aFor a composite thickness of 0.00131 m. This corresponds to a weight gain of 3×10^{-4} kg.

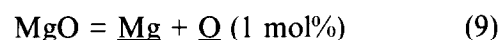
Comparison of the rate of liquid metal transport with the experimental growth rate. The experimental results (Fig. 5) indicate that the weight gain rate decreases with time and is independent of the oxygen pressure. These trends are consistent with a situation where the transport of liquid metal controls the oxidation rate [eqn (7)]. However, the calculated weight gain rate needs to be compared with the experimentally observed value to confirm that the transport of liquid metal through the oxide matrix controls the oxidation rate. The value of $\gamma_{LV} \cos \theta$ in eqn (7) is deduced, as shown in Appendix A. The data used in the calculation of rate based on eqn (7) are shown in Table 3. For a weight gain of 300 mg, which corresponds to a composite thickness of 0.13 cm, the weight gain rate is predicted to be 6415 mg cm⁻² h⁻¹ based on eqn (7), while the experimentally observed weight gain rate is found from Fig. 7 to be 10.8 mg cm⁻² h⁻¹. It is seen that the experimentally observed weight gain rate is about two orders of magnitude lower than the lowest estimate of the predicted weight gain rate (Table 2). Furthermore, the theoretical activation energy for the liquid metal transport corresponds to the temperature sensitivity of viscosity of the liquid aluminium alloy [eqn (7)] and is about 6.1 kJ mol⁻¹,²³ while the experimentally observed value is 361 kJ mol⁻¹. Thus, liquid metal transport through the metal channels does not control the rate of oxidation of Al to Al₂O₃ in the growth stage.

Oxygen transport through alloy film

Flux of oxygen. The flux of dissolved oxygen from the MgO/Al-alloy interface to the Al₂O₃/Al-alloy interface can be estimated using Fick's law as:

$$J = \frac{16D_O(X_O^I - X_O^{II})}{LV_m} \quad (8)$$

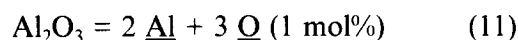
where J denotes the flux of oxygen, D_O is the diffusion coefficient of oxygen in molten aluminium, X_O^I is the mole fraction of dissolved oxygen in the alloy film at the MgO/alloy film interface, X_O^{II} is the mole fraction of dissolved oxygen in the alloy film at the Al₂O₃/alloy film interface, L is the thickness of the alloy film, and V_m is the molar volume of the alloy. The value of X_O^I can be estimated from the MgO/Al-alloy equilibrium:



where $\underline{\text{Mg}}$ and $\underline{\text{O}}$ denote magnesium and oxygen dissolved in the alloy film respectively. From reaction (9) we get:

$$X_O^I = \frac{\exp(-\Delta G_m^0/RT)}{100\gamma_{Mg}X_{Mg}} \quad (10)$$

where ΔG_m^0 is the standard free energy change of reaction (9), X_{Mg} is the mole fraction of magnesium in the aluminium alloy, and γ_{Mg} is the activity coefficient for magnesium in liquid aluminium. A similar expression can be derived for X_O^{II} from the Al₂O₃/Al-alloy equilibrium:



$$X_O^{II} = \frac{\exp(-\Delta G_A^0/3RT)}{100[\gamma_{Al}(1 - X_{Mg})]^3} \quad (12)$$

where ΔG_A^0 is the standard free energy change of reaction (11) and γ_{Al} is the activity coefficient of aluminium in the alloy. It can be seen from eqns (10) and (12) that an increase in the Mg concentration leads to a decrease in the dissolved oxygen concentration at the MgO/alloy interface and an increase in the dissolved oxygen concentration at the Al₂O₃/alloy interface. As a result, the rate of oxygen transport across the alloy film decreases [eqns (8), (10) and (12)]. Thus, with increasing Mg concentration in the alloy film, oxygen transport across the alloy film becomes an important transport step in the growth stage of directed oxidation of Al–Mg alloys.

Oxygen pressure and time dependences of oxygen flux. The Al–Mg alloy in the composite channels attains equilibrium with Al₂O₃/MgAl₂O₄.^{12,16,24} Based on the available thermodynamic data,^{18–20} this equilibrium alloy composition is 0.19 mol% Mg at 1373 K. The Ag–Mg alloy wicks through the metal channels, reacts with the dissolved oxygen and forms fresh alumina epitaxially on the existing alumina. The solubility limit for Mg in Al₂O₃ is 0.012 mol% at 2073 K²⁵ and the solubility decreases rapidly with decreasing temperature. As the

Table 4. Data used in the calculation of oxygen transport through the near-surface alloy layer

Property	Symbol	Value	Ref.
Diffusivity of oxygen in molten aluminium ^a (m ² s ⁻¹)	D_O	1.3×10^{-8}	23
Thickness of alloy layer (m)	L	3×10^{-6}	13
Oxygen concentration in the alloy film at the MgO/film interface ^b (mole fraction)	X_O^I	2.5×10^{-5}	18–20, 27
Oxygen concentration in the alloy film at the Al ₂ O ₃ /film interface ^b (mole fraction)	X_O^{II}	1.1×10^{-6}	18–20, 27

^aTracer diffusivity of oxygen in molten aluminium is approximated by the diffusivity of aluminium in molten aluminium.

^bOxygen concentrations calculated at 1373 K for Mg concentration of 0.19 mol% in the alloy film.

aluminium in the alloy gets oxidized to alumina, the concentration of magnesium in the alloy film tends to increase to values higher than 0.19 mol% Mg. The build-up of magnesium concentration in the alloy film continues with time unless magnesium back-diffusion down the metal channels into the bulk alloy occurs at appreciable rates. Since liquid metal transport through the channels to the reaction interface is fairly rapid, the solute enrichment is likely to continue. It can be seen from eqns (10) and (12) that when the magnesium concentration in the alloy increases, the equilibrium oxygen concentration at the MgO/alloy interface decreases. At the same time, the dissolved oxygen concentration at the Al₂O₃/alloy interface increases. Thus, the increase of magnesium concentration in the alloy film leads to a lower oxygen concentration gradient across the film. As a result, the rate of oxygen transport in the near-surface alloy layer decreases with time. Furthermore, it is observed from eqn (8) that the rate is independent of oxygen pressure. These trends are consistent with the experimentally observed dependence of growth rate on time and oxygen pressure.

As the growth stage progresses, continued Mg enrichment in the near-surface alloy film can lead to the precipitation of MgAl₂O₄ spinel, between the MgO and the underlying metal, as observed by several investigators.^{8,11,26} MgAl₂O₄ forms beneath the MgO rather than on top of Al₂O₃ owing to nucleation considerations.²⁶ The spinel subsequently demixes due to the presence of the oxygen gradient across the alloy film, exposing the film to MgO. A fresh nucleation of Al₂O₃ occurs on the existing alumina layer.^{11,26} This is consistent with the proposed mechanism for the growth stage.

The oxygen required for alumina formation is supplied by dissociation of MgO. The observed continuing decrease in the growth rate with time⁸ is consistent with our proposed model.

Oxygen flux through the near-surface alloy layer and the growth rate. The data used in eqn (8) for calculation of the maximum rate of oxygen transport are presented in Table 4. Note that the oxygen transport rate would be maximum at the start of the growth stage when the Mg concentration in the alloy film corresponds to about 0.19 mol%, i.e. the Mg concentration in the alloy corresponding to the MgAl₂O₄/Al₂O₃ equilibrium at 1373 K. The maximum rate of oxygen transport at 1373 K is estimated to be 53.17 mg cm⁻² h⁻¹. This value is within an order of magnitude of the experimentally observed maximum growth rate of 12.75 mg cm⁻² h⁻¹. The estimated rate of oxygen transport would be exactly equal to the experimental growth rate for a metal layer thickness of about 12 μm. This value of thickness of the metal layer is higher than the values of 1 to 3 μm reported by Antolin *et al.*¹³ However, this value is probably not unreasonable in view of the uncertainties involved in the calculation, and the possibility that the metal layer thickness during the reaction may be higher than that observed after cooling to room temperature. The experimentally determined rate values are consistent with the possibility that oxygen transport through the metal layer is the rate-limiting step in the composite growth stage.

Activation energy of oxygen flux across alloy film.

Since the oxygen concentration at the MgO/alloy film interface is much higher than the dissolved oxygen concentration at the Al₂O₃/metal interface (Table 4), eqn (8) can be approximated as:

$$J = \frac{16D_O X_O^I}{LV_m} \quad (13)$$

Using eqn (10) in (13) we get:

$$J = \frac{16D_O \exp(\Delta H_m^o/RT) \exp(\Delta S_m^o/R)}{100\gamma_{Mg} X_{Mg} LV_m} \quad (14)$$

where ΔH_m^o is the standard enthalpy change for reaction (9) and ΔS_m^o is the standard entropy change for reaction (9). The activation energy for oxygen diffusion in liquid aluminium is small (6.1 kJ mol⁻¹).²³ Therefore, the variation of D_O is insignificant over the temperature range of 1373–1450 K examined in this study. The activation energy for oxygen flux is deduced from eqn (14) as ΔH_m^o , and is equal to 243.6 kJ mol⁻¹.^{18–20,27} Thus, the observed activation energy and weight gain rate in the growth stage are in fair agreement with those predicted for oxygen transport through the near-surface alloy layer. Considerations of the liquid

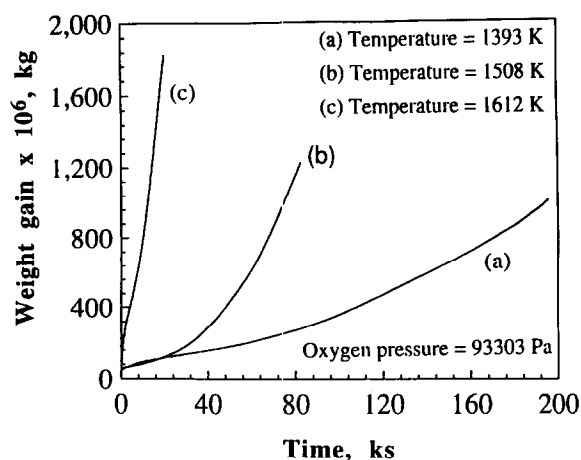


Fig. 8. Weight gain versus time for Al-Mg-Si alloy at different temperatures: (a) 1393 K, (b) 1508 K and (c) 1612 K. The total pressure, oxygen pressure and the total gas flow rate were maintained constant at 93 303 Pa, 93 303 Pa and 8333 mm³ s⁻¹ STP, respectively.

metal transport through channels in the composite or magnesium ion transport through the MgO layer cannot explain the observed oxidation behaviour. The predictions of the oxygen transport model are consistent with the observations of Vlach *et al.*⁸ and Xiao and Derby,¹⁶ who reported parabolic oxidation kinetics in the growth stage and an activation energy of around 270 kJ mol⁻¹. Thus, the transport of oxygen through the near-surface alloy layer is the rate-controlling event in the growth stage of directed oxidation of Al-Mg alloys in the temperature range 1373 to 1450 K.

The proposed model for growth stage kinetics of Al-Mg alloys can be used to predict the effect of additional alloying elements on the growth rate. It is known that Ni additions to Al-Mg alloys refine the composite microstructure.⁵ The effect of Ni additions on the composite growth rate can be predicted with the help of the oxygen transport model. There is a strong interaction between Ni

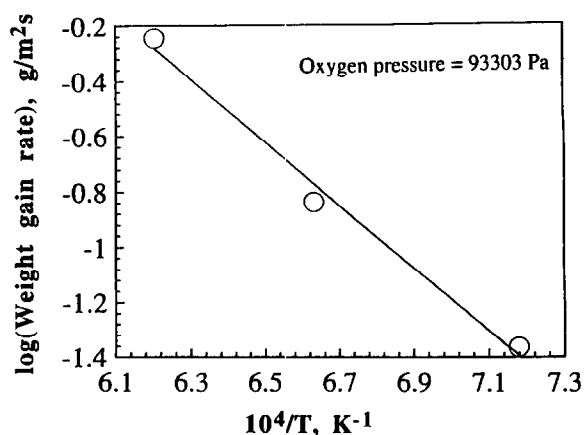


Fig. 9. Weight gain rate versus temperature for Al-Mg-Si alloy for an oxygen pressure of 93 303 Pa. The total pressure and the total gas flow rate were maintained constant at 93 303 Pa and 8333 mm³ s⁻¹ STP, respectively.

Table 5. Growth rate of Al-Mg-Si alloy as a function of oxygen pressure at 1612 K

Oxygen pressure (kPa)	Growth rate (g m ⁻² s ⁻¹)
93.3	0.567
46.6	0.522
23.3	0.439

and Al as indicated by the highly negative heat of formation of Ni-Al intermetallics.²⁰ Therefore, Ni additions to the Al-Mg alloy would be expected to reduce the activity coefficient of Al in the melt. On the other hand, Ni does not form highly stable intermetallics with Mg.²⁰ As a result, Ni would not be expected to influence the Mg activity coefficient in the Al melt. Therefore, it can be seen from eqns (8), (10) and (12) that Ni additions to an Al-Mg alloy would reduce the growth rate. Thus, in addition to refining the composite microstructure,⁵ Ni additions would reduce the composite growth rate.

Mechanism of oxidation of Al-Mg-Si alloys in the growth stage

Figure 8 is a plot of weight gain versus time at various temperatures (1393–1612 K) for an oxygen pressure of 93.3 kPa. The weight gain versus time data in the growth stage in Fig. 8, at a given temperature, could be fitted to a straight line. The average weight gain rates in the growth stage were plotted as a function of temperature in Fig. 9 and the activation energy is found to be 218 kJ mol⁻¹. Weight gain rates were also measured at different oxygen pressures at a temperature of 1612 K (Table 5). The experimental results indicate that the oxidation rate in the growth stage is independent of time and varies as $P_{O_2}^{1/4}$. These trends are consistent with a situation where electronic transport through MgO controls the oxidation rate. This is consistent with the observation of Nagelberg *et al.*¹² that electronic transport controlled the growth rate of Al-Mg-Si alloys. Several important questions arise from the analysis of the data. How does silicon addition to Al-Mg alloy shift the oxidation mechanism from oxygen transport through the near-surface alloy layer to electronic transport through MgO?

Influence of silicon on the oxygen transport through the alloy layer

Formation of Mg-Si clusters in binary Mg-Si liquid solutions²⁸ indicates that silicon additions to Al-Mg alloys could affect the activity of magnesium. The change in the activity of magnesium in the near-surface alloy layer, observed in directed oxidation, would affect the solubility of oxygen at

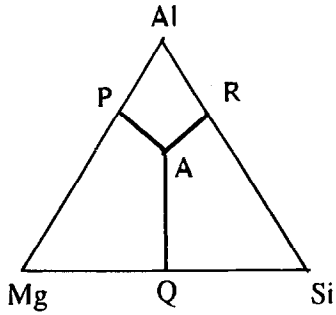


Fig. 10. Schematic description of estimation of Al-Mg-Si thermodynamics from the limiting binaries using the shortest distance composition path. Al-Mg-Si thermodynamics at composition A estimated from the thermodynamics of Al-Mg at composition P, of Mg-Si at composition Q and of Al-Si at composition R, respectively. Compositions P, Q and R were obtained by drawing perpendiculars from A to the three limiting binaries.

the MgO/Al-alloy interface [eqn (10)]. Silicon could also affect the Al activity in the alloy layer. Thus silicon additions are expected to alter the oxygen solubility gradient across the alloy film and, thereby, affect the rate of oxygen transport [eqn (8)]. The effect of silicon additions on the activities of Mg and Al in the near-surface alloy layer can be estimated from Al-Mg-Si ternary liquid solution thermodynamics. Though thermodynamic data on Al-Mg-Si liquid solutions are not available, they can be estimated as shown in Appendix B. The thermodynamics of Al-Mg-Si for the composition A is deduced from the thermodynamics of Al-Mg at composition P, Mg-Si at composition Q and Al-Si at composition R (Fig. 10) by the equation:

$$RT \ln \gamma_{\text{Mg}} = \frac{X_{\text{Al}}^{\text{A}}(X_{\text{Al}}^{\text{A}} + X_{\text{Si}}^{\text{A}})\Delta\bar{G}_{\text{Mg/Al-Mg}}^{\text{XS}}}{(1 - X_{\text{Mg}}^{\text{P}})^2} + \frac{X_{\text{Si}}^{\text{A}}(X_{\text{Al}}^{\text{A}} + X_{\text{Si}}^{\text{A}})\Delta\bar{G}_{\text{Mg/Mg-Si}}^{\text{XS}}}{(1 - X_{\text{Mg}}^{\text{Q}})^2} - \frac{X_{\text{Al}}^{\text{A}}X_{\text{Si}}^{\text{A}}\Delta\bar{G}_{\text{m/Al-Si}}^{\text{XS}}}{X_{\text{Al}}^{\text{R}}X_{\text{Si}}^{\text{R}}} \quad (15)$$

where γ_{Mg} denotes the activity coefficient of Mg in the Al-Mg-Si ternary at the composition A, $\Delta\bar{G}_{\text{Mg/Al-Mg}}^{\text{XS}}$ denotes the excess partial molar free energy of mixing of Mg in the Al-Mg binary at the composition P, $\Delta\bar{G}_{\text{Mg/Mg-Si}}^{\text{XS}}$ denotes the excess partial molar free energy of mixing of Mg in the Mg-Si binary at composition Q, and $\Delta\bar{G}_{\text{m/Al-Si}}^{\text{XS}}$ denotes the excess free energy of mixing of Al-Si binary at composition R. The symbols X_{Al}^{A} , X_{Mg}^{A} and X_{Si}^{A} denote the molar compositions of Al, Mg and Si, respectively, at point A in the Al-Mg-Si ternary diagram. X_{Al}^{P} and X_{Mg}^{P} denote the mole fractions of Al and Mg respectively at composition P, X_{Mg}^{Q} and X_{Si}^{Q} denote the mole fractions of Mg and Si respectively at composition Q, and X_{Al}^{R} and

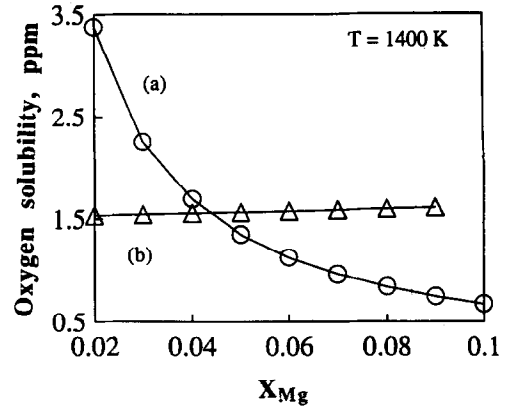


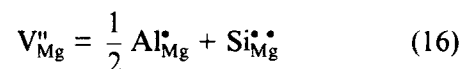
Fig. 11. Calculated equilibrium solubility in the Al-Mg alloy film at (a) the MgO/alloy film interface and (b) the Al_2O_3 /alloy film interface, for varying magnesium contents.

X_{Si}^{R} denote the mole fractions of Al and Si respectively at composition R. Similarly, the activity coefficient of Al in the Al-Mg-Si ternary can be deduced as shown in Appendix B.

Figures 11 and 12 show the effect of Si on the oxygen solubility gradient across the alloy film for Al-Mg and Al-Mg-Si alloys, respectively. It can be observed that the presence of silicon in the melt reduces the oxygen solubility gradient in the alloy film from the MgO/Al-alloy interface to the Al_2O_3 /Al-alloy interface. For the Al-Mg alloy used in this study, SiO_2 additions result in a silicon content in the alloy of 3.3 mol.%. Thermodynamic calculations indicate that silicon addition of 3.3 mol% reduces the activity of Mg in the alloy channels by a factor of 0.67 at a temperature of 1393 K. However, silicon additions do not affect the activity of Al in Al-Mg-Si significantly. Equation (14) indicates that the rate of oxygen transport is inversely proportional to the activity of Mg in the near-surface alloy layer. Thus, for the alloy used in this study, silicon additions accelerate the rate of oxygen transport by a factor of 1.5 at 1393 K. As a result of the enhanced oxygen transport, this step becomes less important in the oxidation of Al-Mg-Si alloys than in that of Al-Mg alloys.

Influence of silicon on electronic transport through MgO

Since silicon is present in the melt, a small proportion would be incorporated into the MgO which is present on top of the near-surface alloy melt. The dissolution of silicon in MgO would increase the concentration of magnesium ion vacancies according to the equation:



where $\text{Si}_{\text{Mg}}^{\bullet}$ represents the dissolved silicon concentration in MgO. It is seen from eqn (16) that silicon

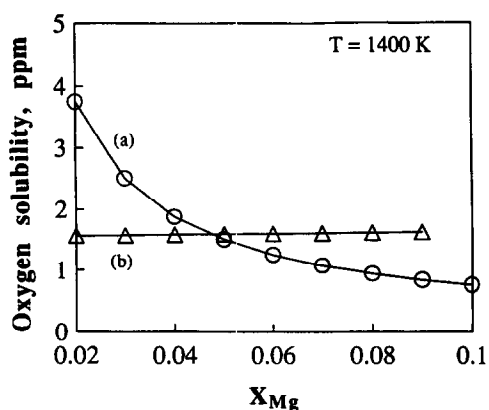


Fig. 12. Calculated equilibrium solubility in the Al-Mg-3.28 wt% Si alloy film at (a) the MgO/alloy film interface and (b) the Al₂O₃/alloy film interface, for varying magnesium contents.

additions increase V_{Mg}^n . Since the hole concentration, p , is inversely proportional to V_{Mg}^n [eqn (4)], silicon additions would thus decrease p . It is known that the rate of electronic transport in MgO is proportional to the hole concentration, p [eqn (6)].¹² As a result, silicon additions to Al-Mg alloys decrease the rate of electronic transport through MgO.

Thus, it is seen that silicon additions to Al-Mg alloys increase the rate of oxygen transport through the alloy film and decrease the rate of electronic transport through MgO, respectively. As a result of the reduced rate of electronic transport through MgO, this step becomes more important in the oxidation of Al-Mg-Si alloys than in that of Al-Mg alloys. The experimental results on the oxygen pressure and time dependences of the growth rate of Al-Mg-Si alloys are consistent with the characteristics of an oxidation reaction controlled by electronic transport through MgO, i.e. growth rate independent of time and proportional to $P_{O_2}^{1/4}$. Thus, the addition of 3.3 mol% Si to Al-5.5 mol% Mg shifts the oxidation mechanism from oxygen transport through the near-surface alloy layer to electronic transport through MgO.

Summary and Conclusions

The oxidation rates in the growth stage of directed oxidation of Al-Mg and Al-Mg-Si alloys have been investigated. The weight gain rate in the growth stage of Al-Mg alloys decreased with time and was independent of oxygen pressure. The activation energy for the growth process was found to be 361 kJ mol⁻¹. The oxygen pressure, time and temperature dependences of the growth rate of Al-Mg alloys are consistent with the characteristics of an oxidation reaction controlled by oxygen transport through the near-surface alloy layer.

The weight gain rate in the growth stage of Al-Mg-Si alloys was independent of time and proportional to $P_{O_2}^{1/4}$. Analysis of the influence of silicon on the various steps in the growth stage indicates that silicon additions increase the rate of oxygen transport through the alloy layer and decrease the rate of electronic transport through the MgO layer. As a result, electronic transport through the outer MgO layer controls the growth stage mechanism in the directed oxidation of Al-Mg-Si alloys, which is consistent with the experimental results. Thus, silicon additions to Al-Mg alloys alter the oxidation mechanism from oxygen transport through the near-surface alloy layer to electronic transport through the MgO layer.

Acknowledgments

The authors wish to thank Dr K. Tankala for useful discussions and Professor R. Roy for his interest in the work. This work was supported by the National Science Foundation, Division of Materials Research under Grant No. DMR-9118075.

References

- Newkirk, M. S., Urquhart, A. W., Zwicker, H. R. & Breval, E., Formation of Lanxide™ ceramic composite materials. *J. Mater. Res.*, **1**[1] (1986) 81-89.
- Venugopalan, H., Tankala, K. & DebRoy, T., Electrical conductivity of alumina/aluminum composites synthesized by directed metal oxidation. *J. Am. Ceram. Soc.*, **77**[11] (1994) 3045-3047.
- Newkirk, M. S., Lesher, H. D., White, D. R., Kennedy, C. R., Urquhart, A. W. & Claar, T. D., Ceramic matrix composites: matrix formation by the directed oxidation of molten metals. *Ceram. Eng. Sci. Proc.*, **8**[7-8] (1987) 879.
- Andersson, C. A., Barron-Antolin, P., Schiroky, G. H. & Fareed, A. S., Properties of fiber-reinforced Lanxide™ alumina matrix composites. *Whisker and Fiber Toughened Ceramics*, ASM International, Materials Park, OH, 1988, pp. 209-215.
- Nagelberg, A. S., Fareed, A. S. & Landini, D. J., Production of ceramic matrix composites for elevated temperature applications using the DIMOX™ directed metal oxidation process. *Processing and Fabrication of Advanced Materials*, The Minerals, Metals and Materials Society, Warrendale, PA, 1992, pp. 127-142.
- Urquhart, A. W., Novel reinforced ceramics and metals: a review of Lanxide's technologies. *Mater. Sci. Eng.*, **A144** (1991) 75-82.
- Nagelberg, A. S., Growth kinetics of Al₂O₃/metal composites from a complex aluminum alloy. *Solid State Ionics*, **32/33**, (1989) 783-788.
- Vlach, K. C., Salas, O., Ni, H., Jayaram, V., Levi, C. G. & Mehrabian, R., A thermogravimetric study of the oxidative growth of Al₂O₃/Al composites. *J. Mater. Res.*, **6**[9] (1991) 1982-1995.
- Venugopalan, H., Tankala, K. & DebRoy, T., Probing the initial stage of synthesis of Al₂O₃/Al composites by directed oxidation of Al-Mg alloys. *Metall. Trans. B*, **27B** (1996) 43-50.

10. Salas, O., Jayaram, V., Vlach, K. C., Levi, C. G. & Mehrabian, R., Early stages of composite formation by oxidation of liquid aluminum alloys. *J. Am. Ceram. Soc.*, **78**[3] (1995) 609–622.
11. Salas, O., Ni, H., Jayaram, V., Vlach, K. C., Levi, C. G. & Mehrabian, R., Nucleation and growth of Al₂O₃/metal composites by oxidation of aluminum alloys. *J. Mater. Res.*, **6**[9] (1991) 1964–1981.
12. Nagelberg, A. S., Antolin, S. & Urquhart, A. W., Formation of Al₂O₃/metal composites by the directed oxidation of molten aluminium–magnesium–silicon alloys: Part II, Growth kinetics. *J. Am. Ceram. Soc.*, **75**[2] (1992) 455–462.
13. Antolin, S., Nagelberg, A. S. & Creber, D. K., Formation of Al₂O₃/metal composites by the directed oxidation of molten aluminum–magnesium–silicon alloys: Part I, Microstructural development. *J. Am. Ceram. Soc.*, **75**[2] (1992) 447–454.
14. DebRoy, T., Bandhopadhyay, A. & Roy, R., Oxide matrix composite by directional oxidation of a commercial aluminum–magnesium alloy. *J. Am. Ceram. Soc.*, **77**[5] (1994) 1296–1300.
15. Standage, A. E. & Gani, M. S., Reaction between vitreous silica and molten aluminum. *J. Am. Ceram. Soc.*, **50**[2] (1967) 101–105.
16. Xiao, P. & Derby, B., Alumina/aluminum composites formed by the directed oxidation of aluminum using sodium hydroxide as a surface dopant. *J. Am. Ceram. Soc.*, **77**[7] (1994) 1771–1776.
17. Manor, E., Ni, H., Levi, C. G. & Mehrabian, R., Microstructure evolution of SiC/Al₂O₃/Al-alloy composites produced by melt oxidation. *J. Am. Ceram. Soc.*, **76**[7] (1993) 1777–1787.
18. Tiwari, B. L., Thermodynamic properties of liquid Al–Mg alloys measured by the emf method. *Metall. Trans. A*, **18A** (1987) 1645–1651.
19. Chase Jr, M. W., Davies, C. A., Bowary Jr, J. R., Fromp, D. J., McDonald, R. A. & Syverud, A. N., *JANAF Thermochemical Tables*, 3rd edn. American Chemical Society, Washington, DC, 1986.
20. Kubaschewski, O., Alcock, C. B. & Spencer, P. J., *Materials Thermochemistry*. Pergamon Press, 1993.
21. Aksay, I., Hoge, C. E. & Pask, J. A., Wetting under chemical equilibrium and non-equilibrium conditions. *J. Phys. Chem.*, **78**[12] (1974) 1778–1783.
22. Brandes, E. A. & Brook, G. B. (eds), *General Physical Properties: Smithells Metals Reference Handbook*, 7th edn. Butterworth-Heinemann, London, UK, 1992, pp. 14–10.
23. Levin, F. S., Polytherms of the viscosity and self-diffusion of molten aluminum. *Izv. Akad. Nauk SSSR, Met.*, **5** (1971) 72–78.
24. Sindel, M., Travitsky, N. A & Claussen, N., Influence of magnesium–aluminum spinel on the directed oxidation of molten aluminum alloys. *J. Am. Ceram. Soc.*, **73**[9] (1990) 2615–2618.
25. Ando, K. & Momoda, M., Solubility of MgO in single crystal Al₂O₃. *J. Ceram. Soc. Jpn, Int. Edn*, **95** (1987) 343–347.
26. Salas, O., Jayaram, V., Vlach, K. C., Levi, C. G. & Mehrabian, R., Banded microstructures in Al₂O₃/Al composites produced by oxidation of molten Al–Mg alloys. In *Processing and Fabrication of Advanced Materials for High Temperature Applications*, eds V. A. Ravi & T. S. Srivatsan. TMS, Warrendale, PA, 1992.
27. Otsuka, S. & Kozuka, Z., Thermodynamic study of oxygen in liquid elements of Group Ib to VIb. *Trans. J. Inst. Met.*, **22**[8] (1981) 558–566.
28. Nayeib-Hashemi, A. A. & Clark, J. B., The magnesium–silicon system. *Bull. Alloy. Phase. Diag.*, **5**[6] (1984) 584–592.
29. Young, T., *Trans. Roy. Soc.*, **95** (1805) 65.
30. Nikolopoulos, P., Surface, grain-boundary and interfacial energies in Al₂O₃ and Al₂O₃–Sn, and Al₂O₃–Co systems. *J. Mater. Sci.*, **20** (1985) 3993–4000.
31. Jacob, K. T. & Fitzner, K., The estimation of the thermodynamic properties of ternary alloys from binary data using the shortest distance composition path. *Thermochim. Acta*, **18** (1977) 197–206.
32. Murray, J. L. & McAlister, A. J., The aluminum–silicon system. *Bull. Alloy. Phase. Diag.*, **5**[1] (1984) 74–84.

Appendix A: Determination of Rate Expression for Liquid Metal Transport

The volumetric flow rate of the liquid alloy through existing capillaries in the composite is given by the Poiseuille equation:

$$\frac{dV}{dt} = \frac{\pi R^4 \Delta P}{8\mu x} \quad (\text{A1})$$

where R is the capillary radius, ΔP is the pressure difference driving the flow, μ is the viscosity of the liquid alloy, and x is the depth of penetration of the liquid at time t . The pressure difference, ΔP , can be represented as:

$$\Delta P = P_c - P_v - P_g \quad (\text{A2})$$

where P_c is the capillary pressure, P_v is the vapour pressure of magnesium in the channel, and P_g is the gravitational pressure due to the weight of the liquid in the channel. The capillary pressure, P_c , driving the flow is given by the expression:

$$P_c = \frac{2\gamma_{LV} \cos \theta}{R} \quad (\text{A3})$$

where γ_{LV} is the surface tension of the liquid aluminium alloy and θ is the contact angle between the liquid Al-alloy and alumina. Exact values of the contact angle, θ , and the surface tension, γ_{LV} , are not available. However, they can be estimated as shown below.

From Young's equation,²⁹ we have

$$\gamma_{LV} \cos \theta = \gamma_{SV} - \gamma_{SL} \quad (\text{A4})$$

where γ_{SV} is the surface energy of alumina and γ_{SL} is the interfacial energy between the molten aluminium alloy and the solid Al₂O₃. Since the metal channels are present in the grain boundaries of alumina,¹ the metal is considered to have spread along the grain boundaries. The condition for metal spreading is given by the following equation:

$$\gamma_{SL} \leq \frac{\gamma_{SS}}{2} \quad (\text{A5})$$

where γ_{SS} is the grain boundary energy in alumina. A lower estimate for $\gamma_{LV} \cos \theta$ is, therefore, given as:

$$\gamma_{LV} \cos \theta = \gamma_{SV} - \frac{\gamma_{SS}}{2} \quad (\text{A6})$$

From eqn (A4) it can be seen that the higher estimate for $\gamma_{LV} \cos \theta$ can be determined by setting γ_{SL} as

zero. The values of γ_{SV} and γ_{SS} can be estimated from the data of Nikolopoulos.³⁰ The lower and the higher estimates for $\gamma_{LV} \cos\theta$ at 1373 K are 0.9455 and 1.4826 J m⁻², respectively.

For the lower estimate of $\gamma_{LV} \cos\theta$, P_c is 9.884 $\times 10^5$ N m⁻² at 1373 K. From Table 3, it is seen that P_g and P_v are much smaller than P_c and are therefore neglected in the determination of ΔP . Therefore, the mass flow rate of Al, (dM/dt) in mol s⁻¹, through a single metal channel is given as:

$$\frac{dM}{dt} = \rho_{Al} \frac{dV}{dt} = \frac{\rho_{Al} \pi R^3 \gamma_{LV} \cos\theta}{4\mu x} \quad (A7)$$

If f is the ratio of the total metal channel area to the area of the composite, the total mass flow rate of Al per unit area of the composite is ($f/\pi R^2$) (dM/dt). Formation of alumina requires 48 g of oxygen for every 54 g of aluminum. Hence the oxygen weight gain rate per unit area, J , is given as:

$$J = \frac{48}{54} f \frac{dM/dt}{\pi R^2} = \frac{48}{54} \frac{f \rho_{Al} R \gamma_{LV} \cos\theta}{4\mu x} \quad (A8)$$

Equation (A1) can be rewritten as:

$$\pi R^2 \frac{dx}{dt} = \frac{\pi R^4 \Delta P}{8\mu x} = \frac{\pi R^3 \gamma \cos\theta}{4\mu x} \quad (A9)$$

Integrating eqn (A9) we get an expression for the depth of liquid penetration, x , as a function of time, t :

$$x = \left[\frac{Rt \gamma_{LV} \cos\theta}{2\mu} \right]^{1/2} \quad (A10)$$

Using the above expression for x in eqn (A8) we get a relation between the flux, J , and the time of oxidation, t :

$$J = \frac{48}{54} f \frac{\rho_{Al}}{4} \left[\frac{2R \gamma_{LV} \cos\theta}{\mu t} \right]^{1/2} \quad (A11)$$

Appendix B: Determination of Al–Mg–Si Liquid Solution Thermodynamics

The thermodynamics of Al–Mg–Si liquid solutions can be estimated from the three limiting binaries (Al–Mg, Mg–Si and Al–Si) using the shortest distance composition path.³¹ The thermodynamics of three limiting binaries (Al–Mg, Mg–Si and Al–Si) is well understood.^{18,28,32} The primary advantage of this technique, over other empirical techniques

used for thermodynamic estimation, is that the binary values incorporated into eqn (15) correspond to the binary compositions closest to the ternary point A (Fig. 10). The excess free energies of mixing for the Al–Mg, Al–Si and Mg–Si binaries can be deduced from experimental data reported in the literature.^{18,28,32} For a given ternary composition A (Fig. 10), X_{Al}^P , X_{Mg}^P , X_{Mg}^Q , X_{Si}^Q , X_{Al}^R and X_{Si}^R can be determined as shown below. These, along with the thermodynamic data of the binaries, can then be incorporated into eqn (15) to determine the activity coefficient of Mg in the Al–Mg–Si ternary.

$$\begin{aligned} X_{Mg}^P &= X_{Mg}^A + \frac{X_{Si}^A}{2} \\ X_{Al}^P &= X_{Al}^A + \frac{X_{Si}^A}{2} \\ X_{Mg}^Q &= X_{Mg}^A + \frac{X_{Al}^A}{2} \\ X_{Si}^Q &= X_{Si}^A + \frac{X_{Al}^A}{2} \\ X_{Al}^R &= X_{Al}^A + \frac{X_{Mg}^A}{2} \\ X_{Si}^R &= X_{Si}^A + \frac{X_{Mg}^A}{2} \end{aligned} \quad (B1)$$

The activity coefficient of Al in the Al–Mg–Si ternary can be similarly estimated from the limiting binaries using the following equation:³¹

$$\begin{aligned} RT \ln \gamma_{Al} &= \frac{X_{Si}^A (X_{Mg}^A + X_{Si}^A) \Delta \bar{G}_{Al/Al-Si}^{XS}}{(1 - X_{Al}^R)^2} \\ &+ \frac{X_{Mg}^A (X_{Mg}^A + X_{Si}^A) \Delta \bar{G}_{Al/Al-Mg}^{XS}}{(1 - X_{Al}^P)^2} \\ &- \frac{X_{Mg}^A X_{Si}^A \Delta G_{m/Mg-Si}^{XS}}{X_{Mg}^Q X_{Si}^Q} \end{aligned} \quad (B2)$$

where γ_{Al} denotes the activity coefficient of Al in the Al–Mg–Si ternary at the composition A, $\Delta \bar{G}_{Al/Al-Mg}^{XS}$ denotes the excess partial molar free energy of mixing of Al in the Al–Mg binary at the composition P, $\Delta \bar{G}_{Al/Al-Si}^{XS}$ denotes the excess partial molar free energy of mixing of Al in the Al–Si binary at composition R, and $\Delta G_{m/Mg-Si}^{XS}$ denotes the excess free energy of mixing of Mg–Si binary at composition Q.